Neurosci. Bull. December, 2019, 35(6):1126–1137
https://doi.org/10.1007/s12264-019-00393-6

www.neurosci.cn
www.springer.com/12264

METHOD

Imaging and Spectral Characteristics of Amyloid Plaque Autofluorescence in Brain Slices from the APP/PS1 Mouse Model of Alzheimer's Disease

Yunling Gao[1] · Qing Liu[2] · Lingling Xu[3] · Ning Zheng[2] · Xiaoming He[4] · Fuqiang Xu[2,5]

Received: 19 October 2018 / Accepted: 12 December 2018 / Published online: 24 May 2019

Abstract Amyloid deposits are one of the hallmark pathological lesions of Alzheimer's disease (AD). They can be visualized by thioflavin-S, silver impregnation, Congo red staining, and immunohistochemical reactions. However, that amyloid deposits generate blue autofluorescence (auto-F) has been ignored. Here, we report that visible light-induced auto-F of senile plaques (SPs) was detected and validated with conventional methods. Brain slices from APP/PS1 (amyloid precursor protein/presenilin 1) transgenic mice were mounted on slides, rinsed, coverslipped and observed for details of the imaging and spectral characteristics of the auto-F of SPs. Then the slices were treated with the above classic methods for comparative validation. We found that the SP auto-F was greatest under blue-violet excitation with a specific emission spectrum, and was much easier, more sensitive, and reliable than the classic methods. Because it does not damage slices, observation of auto-F can be combined with all post-staining techniques in slices and for brain-wide imaging in AD.

Keywords Alzheimer's disease · Amyloid deposits · Senile plaques · Autofluorescence · Spectral imaging · Glial activation

Introduction

Alzheimer's disease (AD) has become one of the most common types of dementia, the most common cause of progressive cognitive decline in the aged population [1]. The clinical hallmarks are progressive impairment of memory, judgment, decision-making, and language [2].

Yunling Gao and Qing Liu have contributed equally to this work.

Electronic supplementary material The online version of this article (https://doi.org/10.1007/s12264-019-00393-6) contains supplementary material, which is available to authorized users.

✉ Qing Liu
liuqing@wipm.ac.cn

✉ Xiaoming He
hxmpumch@163.com

✉ Fuqiang Xu
fuqiang.xu@wipm.ac.cn

[1] Research Section, Xiangyang Central Hospital, Affiliated Hospital of Hubei University of Arts and Science, Xiangyang 441021, China

[2] Center for Brain Science, State Key Laboratory of Magnetic Resonance and Atomic Molecular Physics, National Center for Magnetic Resonance in Wuhan, Key Laboratory of Magnetic Resonance in Biological Systems, Wuhan Institute of Physics and Mathematics, Chinese Academy of Sciences, Wuhan 430071, China

[3] National Center for Magnetic Resonance in Wuhan, State Key Laboratory of Magnetic Resonance and Atomic and Molecular Physics, Wuhan Institute of Physics and Mathematics, Chinese Academy of Sciences, Wuhan 430071, China

[4] Neurology Department, Xiangyang Central Hospital, Affiliated Hospital of Hubei University of Arts and Science, Xiangyang 441021, China

[5] Wuhan National Laboratory for Optoelectronics, Wuhan 430074, China

As one of the pathological hallmark lesions in AD, senile plaques (SPs) can be visualized by several methods, including silver impregnation, Congo red, thioflavin-S (Th-S), and immunohistochemical reactions [3–5]. However, each method has its disadvantages, such as low sensitivity and lack of specificity, and each is also laborious, time-consuming, and variable between tests. Therefore, there are strong incentives to develop more reliable, simple, and inexpensive methods for SP detection. Indeed, these conventional staining techniques have undergone several modifications with the aim of improving their sensitivity, specificity, and reliability. However, that SPs generate blue autofluorescence (auto-F) has been ignored [6–8].

Since the first paper was published in the 1980s, there have been several reports on auto-F from AD-related lesions. The earliest paper by Dowson described SP auto-F in brain tissue from AD patients by irradiating unstained paraffin wax-embedded sections with ultraviolet light [6]. This observation was confirmed by another study on human AD tissue showing that UV light-induced auto-F is restricted to amyloid plaques and is also seen in blood vessels affected by cerebral amyloid angiopathy [7]. In AD model mice, one study has reported that intrinsically fluorescent SPs occurred in acute slices from four different transgenic models [8]. Recently, using cryo-micro-optical sectioning tomography (cryo-MOST), the whole-brain distribution of SP auto-F was visualized in AD transgenic mice [9]. However, so far, SP auto-F has not been widely used, perhaps due to the uncertainty and lack of details of its characteristics. Fortunately, the high sensitivity and resolution of confocal fluorescence microscopy provide the details of SP auto-F, which may be a well-suited and potent diagnostic method for AD. In the present study, we tried to clarify the imaging and spectral characteristics of SP auto-F in brain slices from the APP/PS1 mice.

Materials and Methods

Mice and Tissues

All surgical and experimental procedures were approved by the Animal Care and Use Committee at the Wuhan Institute of Physics and Mathematics, Chinese Academy of Sciences. The experiments were performed on APPswe/PS1ΔE9 (amyloid precursor protein/presenilin 1) mice aged 7–8 months and their wild-type littermates ($n = 6$ mice per genotype), because transgenic mice at this age already show abundant and apparent amyloid deposits. Mice were maintained on a 12/12 h light/dark cycle, and had unrestricted access to food and water. Mice were weighed and deeply anesthetized with urethane (1.4 g/kg i.p.), transcardially perfused with 200 ml saline and then 100 ml 4% paraformaldehyde (PFA) in phosphate-buffered saline (PBS). The brains were post-fixed in 4% PFA at 4°C overnight and then cryoprotected in 30% sucrose solution at 4°C for 72 h. Finally, the brains were cut coronally at 30 μm on a freezing microtome (Leica, CM1850, Nussloch, Germany) and the sections were stored at − 20°C until use.

Autofluorescence Detection

The sections were rinsed in 0.01 mol/L PBS (pH 7.4) for 5 min, mounted on glass slides, dried for 10 min, and mounted with 90% glycerin in PBS. A fluorescence microscope (Olympus, BX-53, Tokyo, Japan) and a laser scanning confocal microscope (LSCM, Leica, TCS SP8 MP, Heidelberg, Germany) were used for SP auto-F detection. Three channels of the BX-53 (U-FUN, BP 360–370, BA 420IF; U-FBW, BP 460–495, BA 510IF; U-FGW, BP 530–550, BA 575IF) and four laser wavelengths on the Leica TCS SP8 MP (405 nm, 488 nm, 552 nm, and 638 nm) were used.

Measurement of Excitation/Emission Spectra

The SP auto-F excitation/emission spectra in the brain sections were measured using the two-photon laser scanning microscope (Leica, TCS SP8 MP) based on a mode-locked laser system operating at 700 nm–1040 nm (equivalent to a single-photon at 350 nm–520 nm) in 20-nm steps. This microscope equipped with a 63 × oil-immersion objective was used to collect the emission fluorescence in the 400 nm–500 nm and 500 nm–600 nm bands. The average laser power on the surface of the samples was maintained at 8.3 mW. The auto-F optical images were processed with ImageJ. To examine the spectrum of the auto-F signal, the shortest wavelength in the single-photon confocal microscope (405 nm) was chosen for the excitation of SPs, and the average laser power on the surface of the samples was maintained at 3.6 μW. The corresponding emission spectra of SPs and nearby control background regions without amyloid deposits were acquired using spectral imaging in the LSCM. For the excitation the lasers passed through a beam splitter BS20/80, and λem was 410 nm–700 nm at 5-nm intervals. After Th-S staining, the emission spectrum for Aβ deposition was scanned with a 488-nm laser. The power was 31 μW under a 63 × objective, and λem was 570 nm–750 nm. The statistics for optical density were calculated with the Leica software, and mapped after normalization with Origin 9.0 software (OriginLab Corporation, Northampton, USA).

Histochemical Staining

For Th-S staining, after auto-F measurements, the coverslips were removed and the sections were washed in 0.01 mol/L PBS (pH 7.4) for 2 min, stained in 1% Th-S (in 50% ethyl alcohol) for 10 min, and then rinsed 3 times in 50% ethyl alcohol for 5 min each. Finally, the slices were mounted with 90% glycerin/PBS.

For modified Bielschowsky's silver staining, after auto-F detection, the coverslips were removed and the slices were rinsed 3 times in ddH_2O for 2 min each, then stained with 3% silver nitrate for 30 min (37°C in the dark). After rinsing 3 times in ddH_2O for 2 min each, sections were reduced for 5 min with 10% formaldehyde until they became light brown and then were rinsed 3 times again. Then the slides were immersed in ammonium silver alcohol solution for 5 min, in 8% formaldehyde until they became dark brown, and then rinsed 3 times. Subsequently, they were immersed in 5% sodium thiosulfate solution for 5 min, dehydrated, cleared, and mounted with xylene-based medium.

For Congo red staining, after auto-F detection, the coverslips were removed and the sections were rinsed in ddH_2O for 2 min, stained in Congo Red solution for 15 min, and then differentiated quickly (10 s) in alkaline alcohol solution. After the sections were washed in ddH_2O for 2 min and counterstained in hematoxylin for 2 min, they were differentiated in 1% hydrochloric acid ethanol for 3 s, and then blued in 0.2% ammonia water for 30 s. Finally, the sections were dehydrated, cleared, and mounted with xylene-based medium.

Immunohistochemistry

Following auto-F detection, the coverslips were removed and the sections were washed in 0.01 mol/L PBS (pH 7.4), then treated with 70% formic acid before triple-labeling immunohistochemistry for Aβ1-16 (1:1000, monoclonal mouse, 6E10, Signet, Dedham, MA, USA), GFAP (1:2000, goat, Abcam, Cambridge, MA, USA), and Iba1 (1:1000, rabbit, Wako, Osaka, Japan). The sections were incubated in 1% bovine serum albumin and 0.2% Triton-PBS for 1 h at room temperature, and finally incubated in diluted primary antibody mixture at 4°C for 24 h. Then after washing 3 times for 5 min each, the sections were incubated with donkey anti-mouse Alexa Fluor 647, donkey anti-rabbit Alexa Fluor 488, and donkey anti-goat Cy3 (Jackson ImmunoResearch, Biomeda, Foster City, CA) for 1 h at 37°C. Two control sections were processed simultaneously. For immunohistochemical detection, negative controls were processed in every immunohistochemistry run.

Quantitative Comparison

Quantitative comparison of the different SP-detecting methods for amyloid plaque area, intensity, and detection rate was done as follows (n = 3 sections for each method). For amyloid plaque area, we chose SPs from the same section before (auto-F) and after one staining method, and compared the relative size of each plaque (area after staining/auto-F area). For amyloid plaque intensity, we also chose SPs from the same section before (auto-F) and after one staining method, measured the intensity of SP auto-F and the background region, and obtained the signal-to-noise ratio ($SNR_{auto\text{-}F}$, intensity of SP auto-F/intensity of background), then the $SNR_{stained}$ of the same plaque after one staining method (intensity of stained SP/intensity of stained background), and calculated the relative intensity ($SNR_{stained}/SNR_{auto\text{-}F}$). For amyloid plaque number, we first checked whether SP auto-F was present when an SP was detected by one of the staining methods, and found that SP auto-F was always present. Then, we checked whether there an SP was detected by one of the staining methods in the same place as SP auto-F, and then calculated the percentage (Detection rate, SP number after one staining method/SP auto-F number). All results are expressed as the mean ± SEM, and the significance of differences was determined by comparison with 1 using the one-sample t-test, A P value < 0.05 was regarded as statistically significant.

Results

Strong Autofluorescence of Senile Plaques Excited by Visible Light

Based on previous reports, we first observed the auto-F in sections of the hippocampus from 7-month-old APP/PS1 transgenic mice under a fluorescence microscope at 360 nm–370 nm excitation (blue-violet) (Fig. 1A). We found that strong blue auto-F was clearly visible against the background fluorescence, exhibiting the characteristic morphology of the "classical" SP with a roughly circular outline and a central core [6]. Furthermore, auto-F was also seen under visible light at other wavelengths (460 nm–495 nm, Fig. 1B, and 530 nm–550 nm, Fig. 1C), but it was very weak and loosely halo-shaped. When we merged the auto-F signals from the three different channels (U-FUN (BP 360–370, BA 420 IF), U-FBW (BP 460–495, BA 510IF), and U-FGW (BP 530–550, BA 575IF)), the densely-packed blue auto-F signal was surrounded by halo-shaped green and red signals, which were almost the same shape (Fig. 1D). Similar auto-F was also seen in

piriform cortex under different wavelengths of visible light (Fig. 1E–H).

In order to check the characteristics of the auto-F images, we observed the same brain sections under the laser scanning confocal microscope. In accordance with the results using the conventional fluorescence microscope, the intensity of the auto-F was maximum when excited at 405 nm under the confocal microscope (Fig. 2A). When the excitation wavelength was increased (from 488 nm to 552 nm and 638 nm), the auto-F still occurred, but with a smaller dense core and a clearer halo than the blue auto-F (Fig. 2B–D). Moreover, when the images acquired at different wavelengths were overlaid, the auto-F signals induced at 488 nm, 552 nm, and 638 nm were very similar (Fig. 2E), but were quite different from that at 405 nm excitation (Fig. 2F).

Before performing more detailed fluorescence confocal microscopy, the excitation spectrum of the auto-F under the two-photon confocal laser scanning microscope was examined (Fig. 2G). We used 700 nm–1040 nm excitation (in 20-nm steps), and collected the emitted light within 400 nm–500 nm and 500 nm–600 nm. We found that the auto-F could be excited within a very broad range, and the strongest emission signal was detected at an excitation wavelength of 700 nm (limited by our two-photon microscope; the continuous excitation wavelength was only from 700 nm to 1040 nm, probably equivalent to 350 nm–520 nm excitation in single-photon microscopy). Moreover, we found that the emission intensity in the 400 nm–500 nm range was higher than that at 500 nm–600 nm for excitation at < 830 nm, but lower for excitation at > 830 nm, indicating that the excitation should be < 830 nm (415 nm in single-photon confocal microscopy) to better detect auto-F. The emission intensity in both ranges decreased as the excitation wavelength increased. In other words, the shorter wavelength the excitation, the stronger the auto-F. Therefore, we chose the shortest excitation wavelength of 405 nm in our single-photon confocal microscope for the following experiments.

Then we collected the 3D images of the auto-F at 405 nm. We obtained continuous images at different foci from the superficial layer to the core of the auto-F, and this showed more clearly that the auto-Fs were irregularly spherical, with an intensely dense core in the center and a faint, loose corona at the surface (Fig. 3A). The auto-F was then identified to be from SPs when the sections were stained with the plaque-specific dye Th-S from both superficial (Fig. 3B, B') and core (Fig. 3C, C') images of the auto-F. We then observed auto-Fs in the brain sections from APP/PS1 mice at different ages (Fig. S1). This showed that, at 3–4 month old, there was no detectable SP auto-F in the dorsal hippocampus, while at 6–7 month, there were some scattered SP auto-Fs, and these showed a significant tendency to increase in number with age, consistent with the previous reports in APP/PS1 mice using conventional staining methods [10].

Source of Senile Plaque Autofluorescence

With regard to the composition of the SP, Miklossy reported that it may reflect the DNA in the SP [11]. To test this, we first captured the auto-F images (Fig. 4A) and then

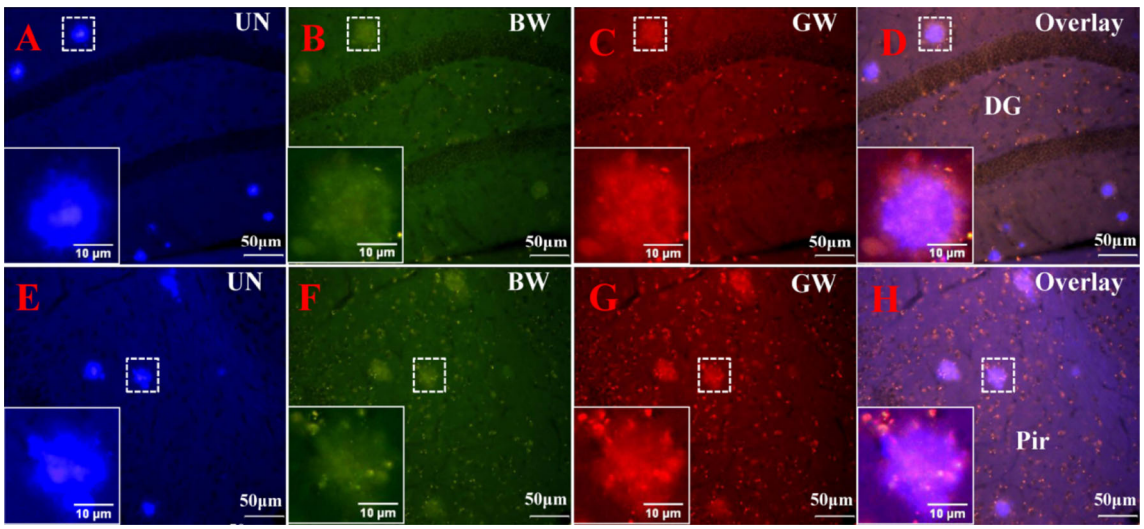

Fig. 1 Autofluorescence (auto-F) detected by visible light in brain slices from APP/PS1 transgenic mice under a conventional fluorescence microscope. **A** Intense blue auto-F was induced in the hippocampus using U-FUN (UN, BP 360–370, BA 420IF). **B**, **C** Only faint auto-F in the hippocampus was excited by U-FBW (BW, BP 460–495, BA 510IF) and U-FGW (GW, BP 530–550, BA 575IF). **D** Overlapped images showing a blue dense core surrounded by halo-shaped green and red signals. **E–H** Amyloid plaque auto-F in piriform cortex under visible light at different wavelengths. Scale bars, 50 μm; insets, 10 μm.

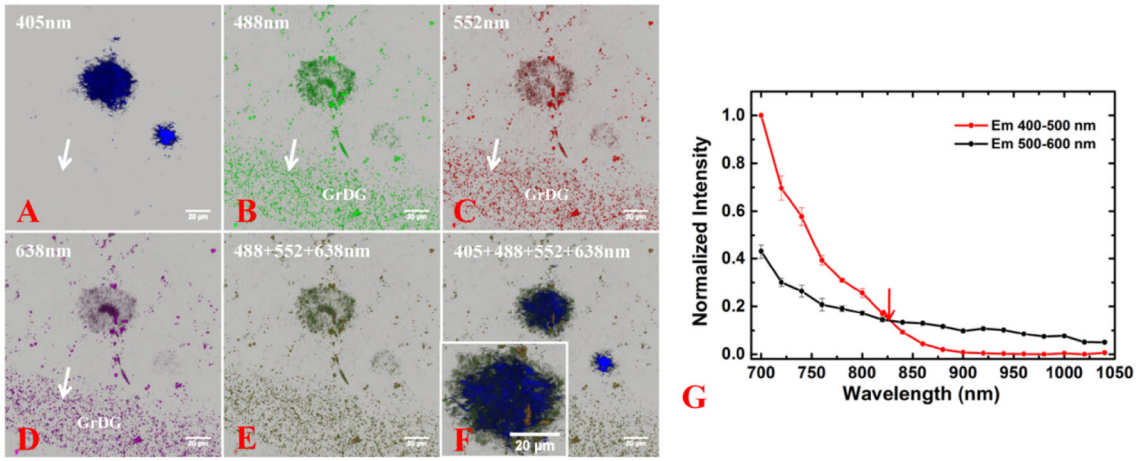

Fig. 2 Auto-F visualized under a laser scanning confocal microscope and their excitation spectra in the AD mouse brain sections. **A**–**F** The intensity of auto-F was maximum at 405 nm excitation (**A**); the plaque core showed strong auto-F, whereas the corona was only faintly fluorescent. As the excitation wavelength increased from 488 nm to 552 nm and 638 nm (**B**–**D**), the SP auto-F showed smaller dense cores and loose halos. They were very similar when overlaid (**E**), but were quite different from that at 405 nm excitation (**F**). **G** Typical excitation spectra of the auto-F in AD mouse brain sections excited from 700 nm to 1040 nm in 20-nm steps using a two-photon confocal microscope. The emission intensity at 400 nm–500 nm (red) and 500 nm–600 nm (black) bands were obtained. Scale bars, 20 μm.

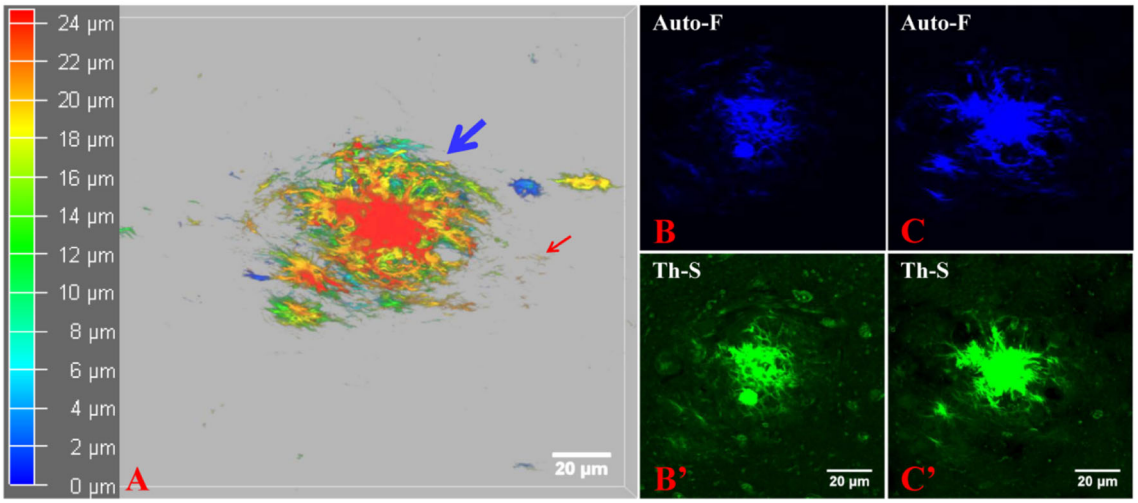

Fig. 3 Auto-F identified to be senile plaques by thioflavin-S staining. The 3D images of auto-F at 405 nm showed that it was irregularly spherical with a dense core and loose halo, which was then identified to be a senile plaque by Th-S staining from both superficial (**B**, **B'**) and core (**C**, **C'**) images of the auto-F. Auto-F, autofluorescence; Th-S, thioflavin-S staining; scale bars, 20 μm.

stained the sections with 4',6-diamidino-2-phenylindole (DAPI), which binds selectively to DNA. We found strongly fluorescent DNA-DAPI complexes in the cell nuclei (Fig. 4B), and the SP auto-F was somewhat weakened after DAPI staining compared with the unstained section (Fig. 4A). Furthermore, we treated the sections with DNase I and found that the fluorescence of the nuclei was decreased (Fig. 4C) with the duration treatment (Fig. S2), but strong fluorescence was still detected in the locations where auto-F had occurred, which were further identified to be SPs with Th-S staining (Fig. 4D).

Then we obtained the emission spectra of SP auto-F. We first measured the emission spectra of the SP and nearby control regions without amyloid deposits excited at 405 nm, and found two peaks of SP auto-F at 440 nm and 465 nm (Fig. 5A, A'). After DAPI treatment, there were still two peaks at ~ 440 nm and 463 nm for SPs, and one peak at ~ 460 nm for the DNA-DAPI complexes (Fig. 5B, B'). After the sections were treated with DNase I for 7 h at 37°C, two similar peaks for SPs and near zero background fluorescence were detected (Fig. 5C, C'). After acquiring the spectra, these sections were stained with Th-S, and the maximum emission wavelengths (λmax) of the emission spectra of the Th-S-stained SP moved to 539 nm and 560 nm (Fig. 5D, D'), distinct from the auto-F emission spectra obtained from unstained sections

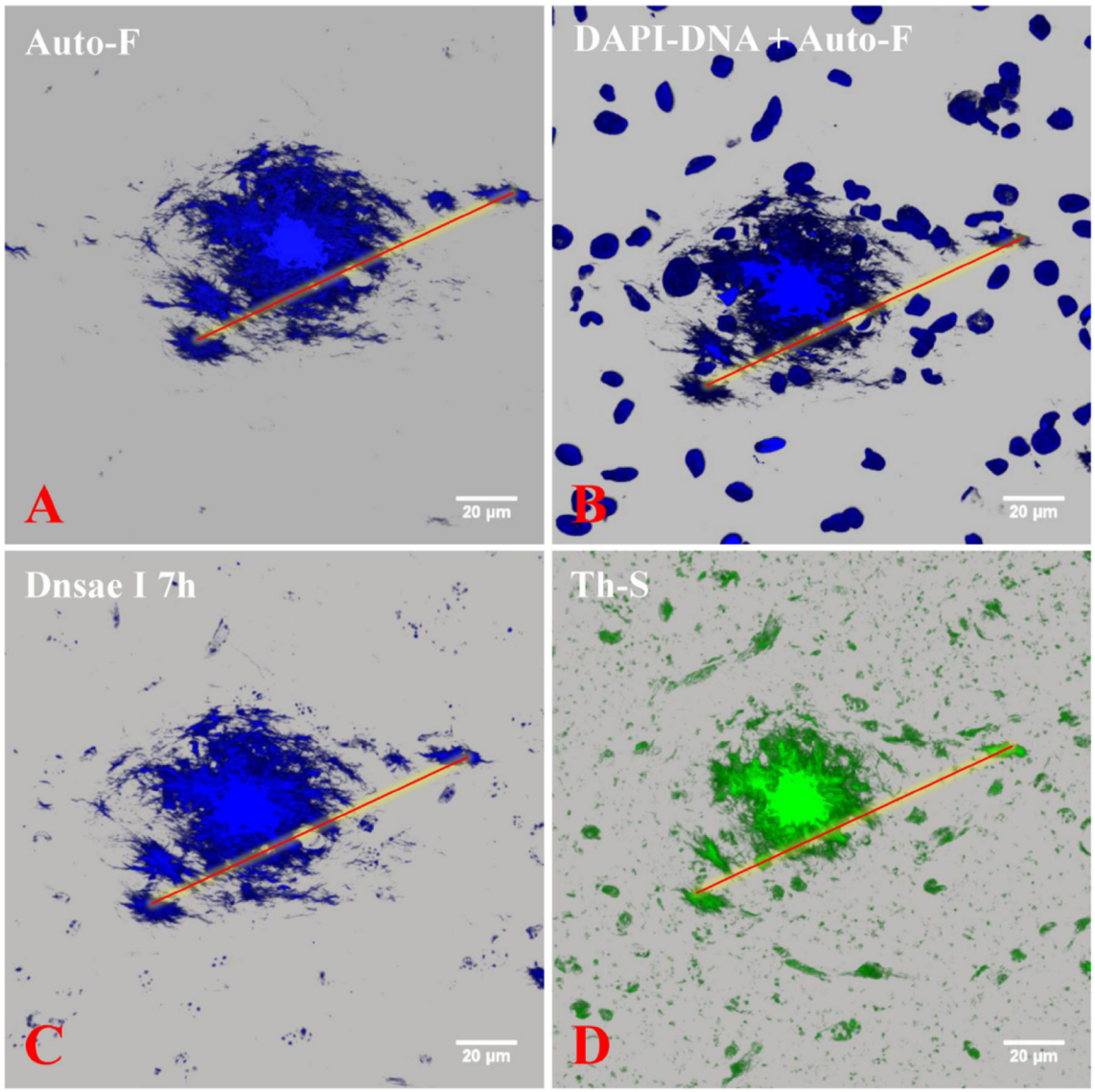

Fig. 4 SP auto-F was not attributable to DNA. **A**, **B** The blue SP auto-F was weakened after DAPI staining compared with the unstained section. **C**, **D** After DNase I treatment, strong blue SP fluorescence still occurred (**C**), which was further confirmed by Th-S staining (**D**), but the fluorescence of the cell nuclei diminished significantly (**C**). Auto-F, autofluorescence; Th-S, thioflavin-S staining; scale bars, 20 μm.

(Fig. 5A, A'). That is to say, the two peaks were both red-shifted by ~ 100 nm. Compared with the untreated SP auto-F, the Th-S-stained SP fluorescence intensity excited at 405 nm became weaker (Fig. 5E'), but that at 488 nm was much stronger (Fig. 5E''), with a shape similar to the blue auto-F excited at 405 nm (Fig. 5E).

Th-S is a dye that fluoresces when it binds to the folds of β-pleated sheet structures. To determine whether the SP auto-F is attributable to the folding of β-pleated sheet structures, we used formic acid treatment, and found that the auto-F of small plaques and fibrous structures almost disappeared, only the auto-F of large dense plagues remaining; this was much smaller but still highlighted (Figs. 6A, B, S3). Then we incubated the sections with 6E10, GFAP, and Iba1 primary antibodies for immunohistochemistry. This showed prominent aggregates of Iba1 expression, with microglial proliferation and activation, and the cell body became hypertrophic, and the processes shortened and gathered around the SP core (Fig. 6C). Also, the GFAP expression remarkably increased in response to amyloid deposits, accompanied by other reactive changes, which included astrocytic hypertrophy, hyperplasia, and process extension surrounding SPs, with some process extended even deep into SPs (Fig. 6D), and the 6E10-positive signal was much broader with a looser periphery (Fig. 6E) than the residual SP auto-F (Fig. 6B). In addition,

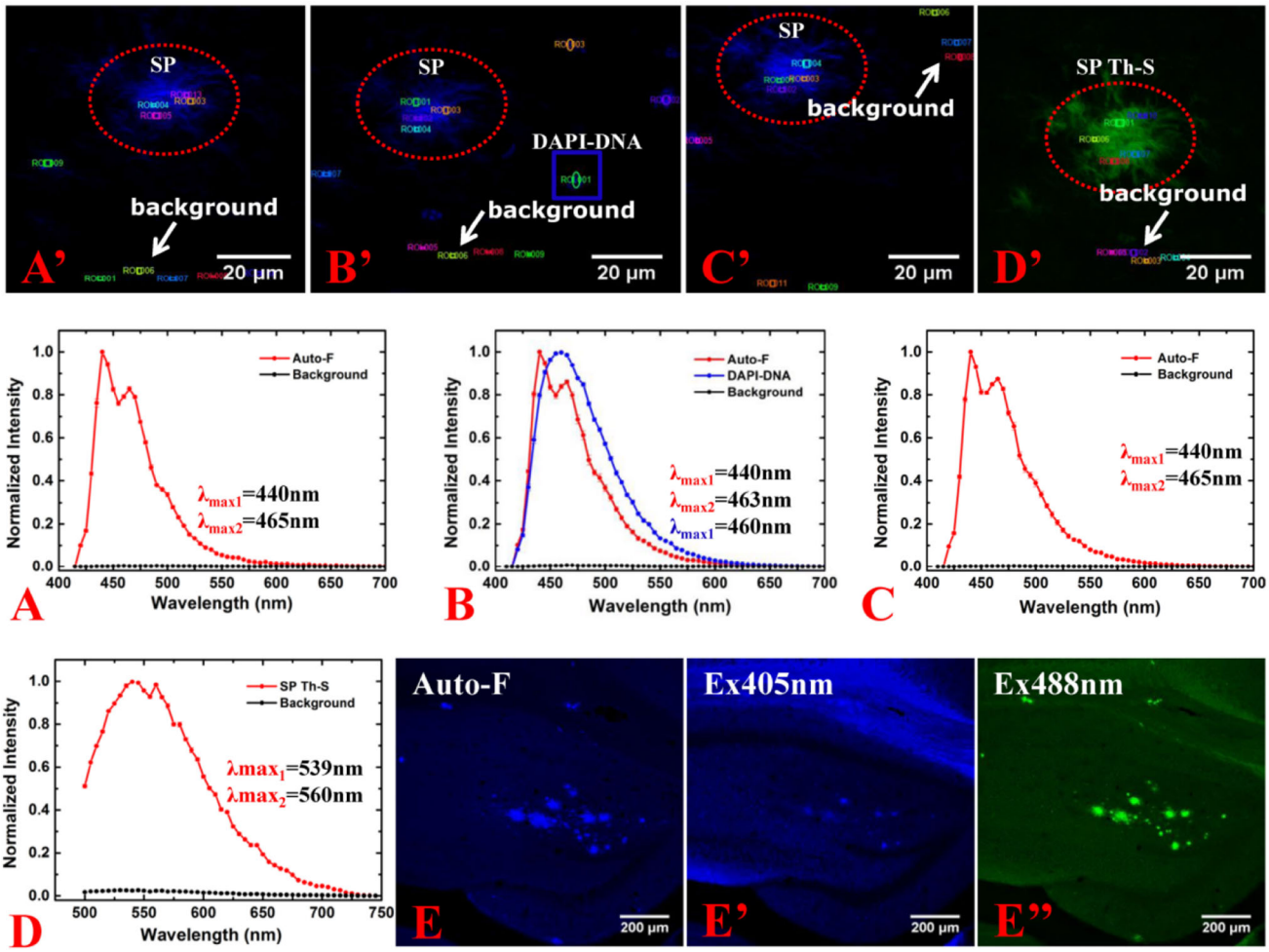

Fig. 5 SP fluorescence emission spectra under different conditions. The SP auto-F spectrum imaging (**A**, **A'**), after DAPI staining (**B**, **B'**), after DNase I treatment (**C**, **C'**), and after Th-S staining (**D**, **D'**). Th-S-stained SP fluorescence excited at 488 nm (**E''**) was significantly brighter than that excited at 405 nm (**E'**) and the auto-F in unstained brain slices (**E**). Ex 405 nm, excited at 405 nm; Ex 488 nm, excited at 488 nm, scale bars, 20 μm (**A'**–**D'**) and 200 μm (**E**–**E''**).

when the four corresponding images were overlaid, it was evident that the auto-F was in the center, the 6E10 signal closely wrapped round with a certain overlap, and then surrounding reactive microglia, and outermost were the activated astrocytes (Fig. 6F).

Comparison of the SP Auto-F with Classical Demonstration Methods

Moreover, we compared the auto-F images with the classical histological staining methods for SPs. We chose three adjacent sections of piriform cortex from APP/PS1 transgenic mice, and observed the SP auto-F in each slice first, then performed modified Bielschowsky's silver staining, Congo red staining, and Th-S staining, separately. We chose three SPs from each section, and found that they showed features different from their auto-F when stained by different methods (Fig. 7) and more details were seen in the magnified images (Fig. S4). The SP auto-F has a high signal-to-background ratio, with loosely distributed fibrous structures surrounding large plaques (Fig. 7A–C). However, after modified Bielschowsky's silver staining, the SPs with strong auto-F still showed strong signals but with a very high background, and the SPs with faint auto-F were even weaker against the high background (Fig. 7A, D). The SPs stained by Congo red showed a strong signal with a relative low background, but were much smaller than the auto-F and might be the core of the SP (Fig. 7B, E). The pattern of SPs stained by Th-S was similar to their auto-F, with a strong signal but also a high background (Fig. 7C, F).

We then quantitatively compared the different SP-detecting methods in terms of amyloid plaque area, intensity, and detection rate (Table 1). The results showed significant differences between auto-F and these conventional staining methods in area (relative size, all $P < 0.01$);

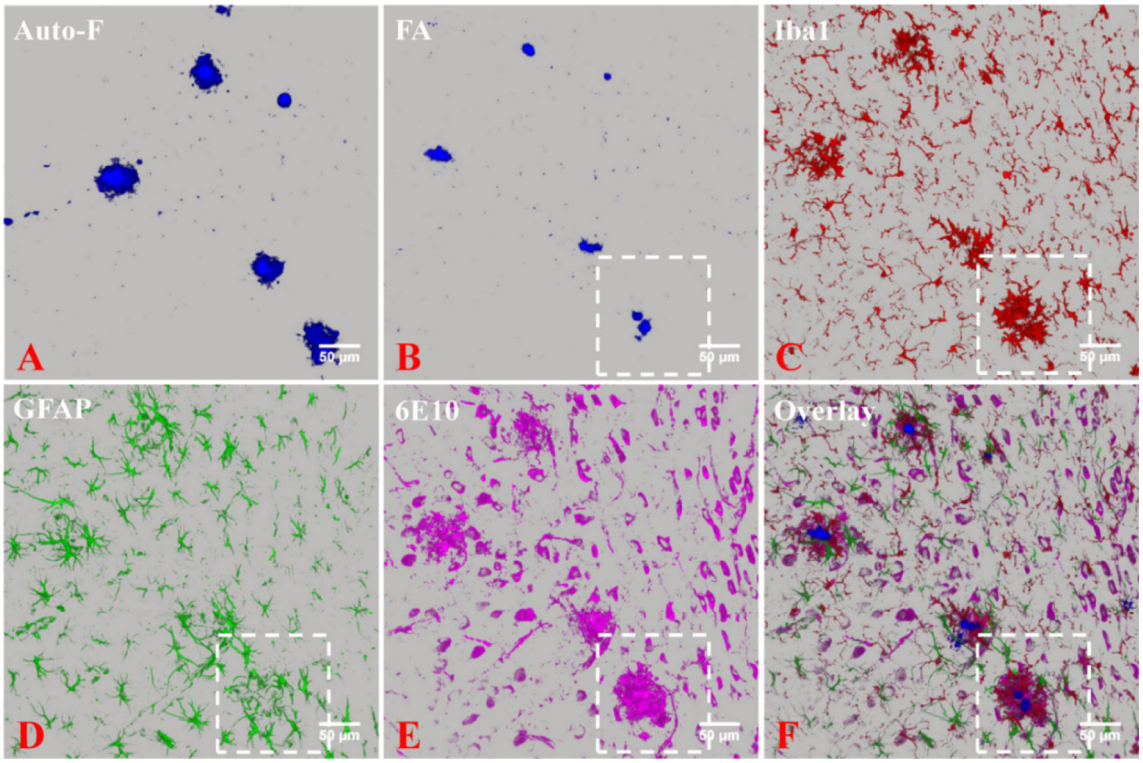

Fig. 6 Relationships between amyloid deposits and reactive microglia and astrocytes. Brain sections were pretreated with formic acid, and then triple-labeled with 6E10, GFAP, and Iba1 for immunohistochemistry. The SP auto-F was diminished after formic acid treatment (**A**, **B**). The Iba1- (**C**), GFAP- (**D**), and 6E10-positive (**E**) signals all occurred in the vicinity of SP auto-F. When the images were overlaid, it was evident that the auto-F was in the center, then the 6E10 signal was closely wrapped round with a certain overlap, then surrounding reactive microglia, and outermost were the activated astrocytes (**F**). FA, formic acid; scale bars, 50 μm.

Table 1 Characteristics of senile plaques detected by different staining methods relative to autofluorescence.

Method	Relative size	*P*	Relative intensity	*P*	Detection rate	*P*
Th-S	0.73 ± 0.03	< 0.001***	1.07 ± 0.02	< 0.001***	0.99 ± 0.01	0.391
Congo Red	0.59 ± 0.03	< 0.001***	0.28 ± 0.01	< 0.001***	0.88 ± 0.01	< 0.001***
Silver stain	2.62 ± 0.48	< 0.01**	0.25 ± 0.01	< 0.001***	0.56 ± 0.02	< 0.05*
6E10	2.63 ± 0.22	< 0.001***	0.89 ± 0.04	< 0.01**	0.94 ± 0.01	< 0.05*

Data shown as mean ± SEM.

**$P < 0.05$; **$P < 0.01$; ***$P < 0.001$.

the SP auto-F had enough signal-to-noise ratio to be visible, much higher than that after Congo red, silver staining, and 6E10 immunohistochemistry (relative intensity, all $P < 0.01$); and the SP auto-F had a detection rate similar to that after Th-S staining, much higher than that after Congo red, silver staining, and 6E10 immunohistochemistry (all $P < 0.05$).

Besides amyloid plaques, cerebral amyloid angiopathy is another pathological hallmark in AD patients. We observed the auto-F in sections with cortical vessel walls, cortex, and pia mater under blue-violet light, and found evident auto-F in all these areas (Fig. 8A, B), but not in control mouse brain (Fig. 8C). The auto-F in cortical vessel walls and pia mater, which had thick plate-like aggregates (Fig. 8A', A'', B'), was quite different from the spherical auto-F in cortex. To further confirm that the auto-F was specifically from the amyloid deposits, after auto-F detection (Fig. 8D), the sections were stained with Th-S (Fig. 8E), and the results showed that the auto-F in cortical vessel walls and pia mater were indeed amyloid deposits.

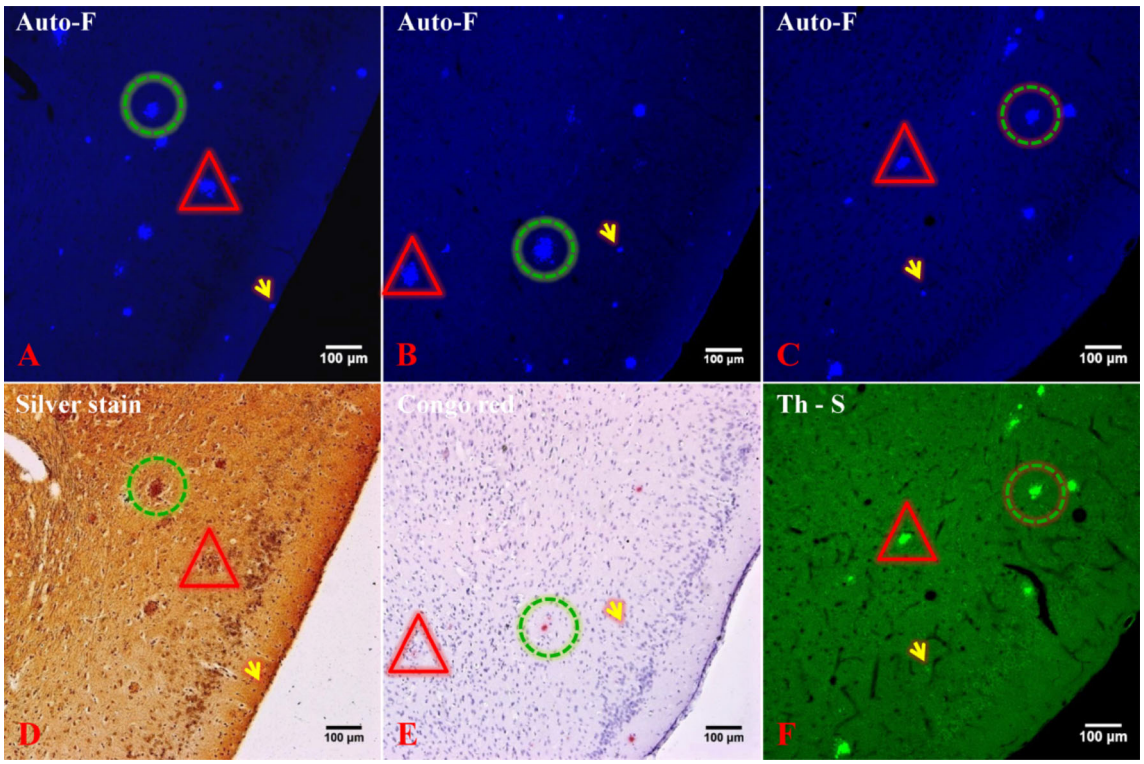

Fig. 7 Comparison of modified Bielschowsky's silver staining, Congo red staining, and Th-S staining with auto-F images of SP. SPs had a low signal-to-noise ratio with very high background after modified Bielschowsky's silver staining (**A**, **D**). SPs were much smaller with a low signal-to-noise ratio after Congo red staining (**B**, **E**), and were similar to their auto-F images with a high signal-to-noise ratio after Th-S staining (**C**, **F**). Auto-F, autofluorescence; Th-S; thioflavin-S staining; scale bars, 100 μm.

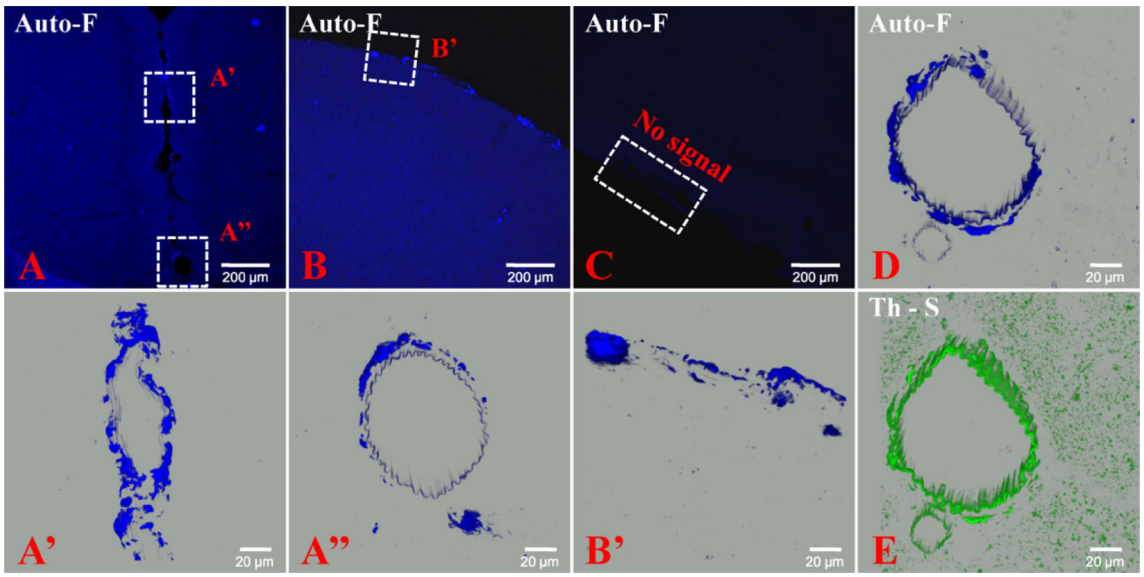

Fig. 8 SP auto-F in sections from AD mouse brain with cortical vessel walls, cortex, and pia mater at 405 nm excitation (**A**, **B**), and no SP auto-F was detected in control mice (**C**). The magnified horizontal (**A'**), coronal (**A"**), and surrounding (**B'**) images showed thick plate-like aggregations that were identified with Th-S (**D**, **E**). Auto-F, autofluorescence; Th-S, thioflavin-S; scale bars, 200 μm (**A**–**C**), 20 μm (**A'**, **A''**, **B'**, **D**, **E**).

Discussion

Since the first description of the auto-F of amyloid deposits in the 1980s [6], auto-F detection has undergone several modifications with the aim of improving sensitivity, specificity, and reliability [7, 8]. However, it has not been commonly used yet, perhaps due to the uncertainty and the limited knowledge of SP auto-F.

Consistent with previous reports, in this study we visualized the auto-F elicited by visible light under a conventional fluorescence microscope in brain sections from APP/PS1 transgenic mice (Fig. 1), and found morphology similar to "classical" SPs [6]. To define the details of the SP auto-F, we further observed them under a laser scanning confocal microscope and analyzed the excitation spectrum of the auto-F (Fig. 2). We found that, in accord with previous reports, the most evident auto-F was excited under the shortest wavelength in our confocal microscope, 405 nm (Fig. 2). They showed a characteristic strong and clear blue signal against the background, irregularly spherical with an intense core and loose corona. The auto-F was then identified to be amyloid deposits by Th-S staining (Fig. 3). Furthermore, we found that DNase I treatment did not significantly affect the SP auto-F (Fig. 4), and analyzed the emission spectrum of SP excited at 405 nm (Fig. 5). However, with formic acid pretreatment, the SP auto-F was significantly diminished (Fig. 6). Therefore, the auto-F was from β-pleated sheet amyloid deposits composed of proteins with very different primary amino-acid sequences. In consequence, this property makes it very useful in studying cerebral and systemic amyloidosis as we found in cortical vessel walls, cortex, and pia mater (Fig. 8).

The Material and Structural Basis of Senile Plaque Autofluorescence

With regard to the details of SP auto-F, it has been reported that the fluorescence of SPs stained with DAPI is due to the DNA they contain [11]. Staining with DAPI is a common method for the detection of DNA, so we used DNase I to digest DNA and found that after the cell nucleus disappeared, the fluorescence of the SPs remained (Fig. 4), showing that the SP auto-F cannot be attributed to DAPI-DNA complexes. Moreover, we found that the excitation spectrum of SP auto-F and DAPI-DNA complexes under violet light had one peak in common at $\sim$ 460 nm (Fig. 5), which might be the reason for the previous conclusion that DNA in SPs emits the fluorescence. Then the auto-F was identified to be from amyloid deposits by staining with Th-S, and both the excitation and emission spectra had been red-shifted with the pattern unchanged (Fig. 5), indicating that, the conformation of the SP changes when it combines with Th-S. So we confirmed that it is not the DNA in SP that emits the fluorescence, but the aggregated amyloid deposits are the material basis of the SP auto-F. In our study, the SP auto-F was also overlaid with the 6E10-positive signal, which is consistent with the previous report that full-length Aβ exhibits auto-F, but not the N-terminal-truncated Aβ deposits [7].

Furthermore, our study showed that SP auto-F was strong and clearly detectable with a characteristic emission spectrum with peaks at 440 nm and 463 nm at 405-nm excitation (Fig. 5), implying that there are two chemical compounds, or the structure of one chemical changes in response to Aβ pathology causing a shift of the emission spectrum. Then, we found that the SP auto-F was diminished by formic acid pretreatment (Fig. 6). Because formic acid immediately destroys the secondary structure of proteins (β-pleated sheet structure) without cleaving or removing the protein, so the SP auto-F was due to their secondary structure, which is the structural basis of the SP auto-F.

It was interesting to note that the auto-F of amyloid deposits at 405 nm had two emission peaks (440 nm and 463 nm), and Warren (2003) found in AD patients at autopsy that neurofibrillary tangles have very strong auto-F and a single emission peak at 460 nm [12]. Whether the SP auto-F detected under the 405 nm laser has the same components as neurofibrillary tangles needs further investigation.

Advantages of Auto-F Over Classical Methods of Detecting Amyloid Deposits

Here, we compared different staining methods with SP auto-F. The SP auto-F signal manifested a densely-highlighted core and loosely-distributed fibers (Figs. 1, 2, 3). However, the SP images after different staining methods had different characteristics (Table 1). The signal-to-noise ratio of SPs was significantly lower, with a very high background, after modified Bielschowsky's silver staining. This ratio was also not high after Congo red staining, perhaps only showing the core of the SP. The pattern of SPs stained by Th-S was quite similar to their auto-F, with a high signal-to-noise ratio despite a stronger background. Thus, auto-F allows the specific recognition of amyloid deposits when excited by blue and violet light, whereas classical staining visualization is not so sensitive. With regard to detecting the presence of Aβ-deposits in a given case, the sensitivity and specificity of auto-F detection were 100% in our study. Auto-F observation was the most reliable among the methods we used and provided an almost selective demonstration of amyloid

deposits. Of more importance is that this method is simple and the cost is very low.

Moreover, we detected Aβ deposits with the 6E10 antibody, together with plaque-associated glial responses as previously reported [13]. We found that the 6E10 signal was much broader with a looser periphery than the SP auto-F dense core after formic acid treatment. It is worth noting that in our study, amyloid plaques were typically surrounded by activated microglia and then astrocytes in sequence, consistent with the recent report that neurotoxic reactive astrocytes are induced by activated microglia [14]. Longitudinal imaging has shown that amyloid plaques develop surprisingly rapidly and microglia become reactive and are attracted to the sites of plaque formation within 24 h [15]. However, the roles of microglia and astrocytes in the AD process remain controversial. Some studies have suggested that microglia play protective roles, while others have suggested that microglia cause secondary neuronal injury [16]. It has also been reported that astrocytes and microglia communicate with each other and this cross-talk is important in promoting glial activation [17]. Moreover, the microglial response to dense-core plaques is proportional to plaque size, while the astrocytic response is not correlated with plaque size [18]. Another report showed that microglia act as a barrier that restricts the radial expansion of plaques, and induce reactive astrocytes, which could drive neurodegeneration [19]. Our results support the idea that microglia are first recruited and then astrocytes are chemotactic to amyloid deposits.

Application Prospects of SP Auto-F Observation

Previously, identification of Aβ, the major component of senile plaques, in brain tissue was limited to static histological approaches, such as silver staining, Congo red staining, Th-S staining, and immunohistochemical methods. Compared with these conventional methods of pathological examination for amyloid deposition, auto-F detection has absolute advantages: clear, specific, and direct-viewing images can be obtained without any staining of the specimen, so it can be used as a pre-protocol to either specific staining or the immunohistochemical operations on brain slices for SPs and cerebral amyloid angiopathy.

Moreover, multiphoton microscopy has become an increasingly important tool for imaging the structures and functions of the living brain. It has been widely used in preclinical studies of animal models of AD, because it is minimally invasive, provides high resolution, and can be performed repeatedly in the same animal. It has already been used to observe the dynamic progression of Aβ aggregation in amyloid plaques and cerebral amyloid angiopathy after staining in real-time in transgenic mouse models of AD [20, 21], which can help us to understand the pathogenesis and pathogenicity of amyloid plaques in the context of AD. Moreover, SP auto-F observation in acute brain slices from AD transgenic mice has been demonstrated using multiphoton microcopy combined with second harmonic generation microscopy [8], and brain-wide visualization of SP auto-F in AD transgenic mice has been achieved using cryo-MOST [9]. Furthermore, although microdissection of amyloid plaques after Th-S staining has proved an effective method to demarcate amyloid plaques for excision [22], auto-F can be better used to selectively dissect SPs, and then fluorescent laser capture microdissection combined with liquid chromatography-mass spectrometry can be used to identify components in amyloid plaques. Given that there were distinct differences between the SP auto-F and that after Th-S staining, SPs dissected on the basis of auto-F could be more reflective of their nature.

Auto-F observation, with no need for staining, causing no damage to the samples, and keeping the morphology and metabolic activity at a maximum, may be an ideal way to detect AD pathology both *in vitro* and *in vivo*. We anticipate that this work will be useful for paving the way to using auto-F signals to investigate the pathological mechanisms in AD.

Acknowledgements This work was supported by the National Natural Science Foundation of China (31771156 and 31400945).

Conflict of interest The authors claim that there are no conflicts of interest.

References

1. Ferrari C, Lombardi G, Polito C, Lucidi G, Bagnoli S, Piaceri I, *et al.* Alzheimer's disease progression: factors influencing cognitive decline. J Alzheimers Dis 2018, 61: 785–791.
2. Blennow K, de Leon MJ, Zetterberg H. Alzheimer's disease. Lancet 2006, 368: 387–403.
3. Navarro A, del Valle E, Martinez E, Ordonez C, Perez C, Tolivia J. Highly selective and fast diagnosis of Alzheimer's disease hallmark lesions using congo red in isopropyl alcoholic solution. J Alzheimers Dis 2013, 35: 589–597.
4. Mavrogiorgou P, Gertz HJ, Ferszt R, Wolf R, Bar KJ, Juckell G. Are routine methods good enough to stain senile plaques and neurofibrillary tangles in different brain regions of demented patients? Psychiatr Danub 2011, 23: 334–339.
5. Wisniewski HM, Wen GY, Kim KS. Comparison of four staining methods on the detection of neuritic plaques. Acta Neuropathol 1989, 78: 22–27.
6. Dowson JH. A sensitive method for the demonstration of senile plaques in the dementing brain. Histopathology 1981, 5: 305–310.
7. Thal DR, Ghebremedhin E, Haass C, Schultz C. UV light-induced autofluorescence of full-length Abeta-protein deposits in the human brain. Clin Neuropathol 2002, 21: 35–40.
8. Kwan AC, Duff K, Gouras GK, Webb WW. Optical visualization of Alzheimer's pathology via multiphoton-excited intrinsic

fluorescence and second harmonic generation. Opt Express 2009, 17: 3679–3689.
9. Luo Y, Wang A, Liu M, Lei T, Zhang X, Gao Z, *et al.* Label-free brainwide visualization of senile plaque using cryo-micro-optical sectioning tomography. Opt Lett 2017, 42: 4247–4250.
10. Wang H, He J, Zhang R, Zhu S, Wang J, Kong L, *et al.* Sensorimotor gating and memory deficits in an APP/PS1 double transgenic mouse model of Alzheimer's disease. Behav Brain Res 2012, 233: 237–243.
11. Miklossy J. Bacterial amyloid and dna are important constituents of senile plaques: further evidence of the spirochetal and biofilm nature of senile plaques. J Alzheimers Dis 2016, 53: 1459–1473.
12. Zipfel WR, Williams RM, Christie R, Nikitin AY, Hyman BT, Webb WW. Live tissue intrinsic emission microscopy using multiphoton-excited native fluorescence and second harmonic generation. Proc Natl Acad Sci U S A. 2003, 100: 7075–7080.
13. Yang JT, Wang ZJ, Cai HY, Yuan L, Hu MM, Wu MN, *et al.* Sex differences in neuropathology and cognitive behavior in APP/PS1/tau triple-transgenic mouse model of Alzheimer's disease. Neurosci Bull 2018, 34: 736–746.
14. Liddelow SA, Guttenplan KA, Clarke LE, Bennett FC, Bohlen CJ, Schirmer L, *et al.* Neurotoxic reactive astrocytes are induced by activated microglia. Nature 2017, 541: 481–487.
15. Meyer-Luehmann M, Spires-Jones TL, Prada C, Garcia-Alloza M, de Calignon A, Rozkalne A, *et al.* Rapid appearance and local toxicity of amyloid-beta plaques in a mouse model of Alzheimer's disease. Nature 2008, 451: 720–724.
16. Edison P, Donat CK, Sastre M. In vivo imaging of glial activation in Alzheimer's disease. Front Neurol 2018, 9: 625.
17. Bouvier DS, Murai KK. Synergistic actions of microglia and astrocytes in the progression of Alzheimer's disease. J Alzheimers Dis 2015, 45: 1001–1014.
18. Serrano-Pozo A, Muzikansky A, Gomez-Isla T, Growdon JH, Betensky RA, Frosch MP, *et al.* Differential relationships of reactive astrocytes and microglia to fibrillar amyloid deposits in Alzheimer disease. J Neuropathol Exp Neurol 2013, 72: 462–471.
19. Condello C, Yuan P, Schain A, Grutzendler J. Microglia constitute a barrier that prevents neurotoxic protofibrillar Aβ42 hotspots around plaques. Nat Commun 2015, 6:6176.
20. D'Amore JD, Kajdasz ST, McLellan ME, Bacskai BJ, Stern EA, Hyman BT. In vivo multiphoton imaging of a transgenic mouse model of Alzheimer disease reveals marked thioflavine-S-associated alterations in neurite trajectories. J Neuropathol Exp Neurol 2003, 62: 137–145.
21. Dong J, Revilla-Sanchez R, Moss S, Haydon PG. Multiphoton in vivo imaging of amyloid in animal models of Alzheimer's disease. Neuropharmacology 2010, 59: 268–275.
22. Nijholt DA, Stingl C, Luider TM. Laser capture microdissection of fluorescently labeled amyloid plaques from Alzheimer's disease brain tissue for mass spectrometric analysis. Methods Mol Biol 2015, 1243: 165–173.